

# Observation-dependent Bayesian active learning via input-warped Gaussian processes

Sanna Jarl<sup>\*1,2</sup> Maria Båkestad<sup>\*2</sup> Jonathan J. S. Scragg<sup>3</sup> Jens Sjölund<sup>1</sup>

## Abstract

Bayesian active learning relies on the precise quantification of predictive uncertainty to explore unknown function landscapes. While Gaussian process surrogates are the standard for such tasks, an underappreciated fact is that their posterior variance depends on the observed outputs only through the hyperparameters, rendering exploration largely insensitive to the actual measurements. We propose to inject observation-dependent feedback by warping the input space with a learned, monotone reparameterization. This mechanism allows the design policy to expand or compress regions of the input space in response to observed variability, thereby shaping the behavior of variance-based acquisition functions. We demonstrate that while such warps can be trained via marginal likelihood, a novel self-supervised objective yields substantially better performance. Our approach improves sample efficiency across a range of active learning benchmarks, particularly in regimes where non-stationarity challenges traditional methods.

## 1. Introduction

The efficient exploration of unknown, expensive functions remains a central challenge at the intersection of Bayesian inference and sequential decision-making (Krause & Guestrin, 2007; Ghavamzadeh et al., 2015). In the context of black-box optimization and active learning, Bayesian Optimization (Garnett, 2023) has emerged as a de facto standard, providing a principled framework for sequential exploration and exploitation via a probabilistic surrogate—most commonly a Gaussian process (GP) (Rasmussen & Williams,

<sup>\*</sup>Equal contribution <sup>1</sup>Department of Information Technology, Uppsala University, Uppsala, Sweden <sup>2</sup>Department of Computer Science, RISE Research Institute of Sweden, Stockholm, Sweden <sup>3</sup>Department of Solar Cell Technology, Uppsala University, Uppsala, Sweden. Correspondence to: Sanna Jarl <sanna.jarl@angstrom.uu.se>.

Preprint. February 3, 2026.

2006). The efficacy of this paradigm relies on the surrogate’s ability to accurately quantify uncertainty, which, in turn, guides acquisition functions to regions of the search space most likely to yield informative observations.

However, a fundamental structural limitation exists in the standard GP formulation: the posterior variance, and by extension any variance-based acquisition strategy, is conditionally independent of the observed function values  $y$  given the input locations (Krause et al., 2008). While this algebraic property simplifies the computation of information gain, it decouples the exploration logic from the observed complexity of the objective function. Consequently, under fixed hyperparameters, a traditional GP-based agent operates as an open-loop system: the sequence of queries is determined entirely by the geometry of the input locations, rather than by feedback from the observed function values. This leads to a common failure mode in scientific discovery, where the agent remains oblivious to regions of high volatility until they are serendipitously sampled (Teixeira Parente et al., 2023; Jarl et al., 2025).

To address this limitation, we propose an input-warped Gaussian process framework in which the geometry of the input space is adaptively reparameterized to reflect observed function variability during exploration, as illustrated in Figure 1. Crucially, we decouple prediction from exploration: a stationary GP surrogate is retained for modeling and evaluation, while a learned nonlinear input reparameterization is used exclusively within the acquisition function. This separation allows observed data to influence exploration through geometry, without altering the underlying probabilistic model.

We instantiate the reparameterization using conditional rational quadratic splines (Durkan et al., 2019), which define smooth, monotone transformations of the input space. The resulting warp adapts locally to the structure of the target function, expanding regions of rapid variation and compressing smoother regions. This reshaping alters the geometry used to evaluate predictive variance, making variance-based acquisition sensitive to function complexity under otherwise stationary kernels. Although the warp can be learned by maximizing the marginal likelihood, we instead introduce a self-supervised training objective that more directly reflects the requirements of exploration.

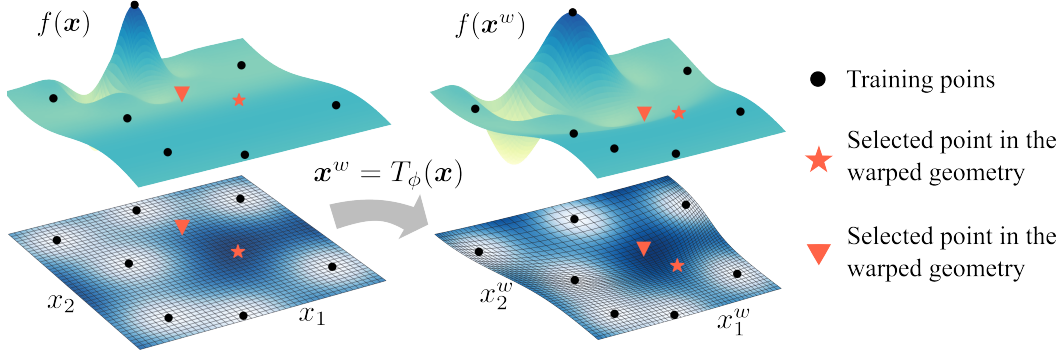


Figure 1. An example demonstrating the necessity of warping the input space. On the left, we see the scenario of an unwarped GP, on the right, a warped GP with the locations of two selected new points. We see that complex regions are stretched out, while flatter regions are compressed, facilitating the selection of points in complex regions.

In summary, our contributions are threefold: (i) we show the geometric nature of variance-based acquisition and its resulting open-loop behavior under stationary Gaussian process models; (ii) we introduce a decoupled acquisition framework that learns an input reparameterization used solely for exploration, leaving prediction unchanged; and (iii) we propose a self-supervised geometric training objective that is better aligned with the goals of active learning than marginal likelihood maximization.

## 2. Background

The problem of sequentially selecting data to efficiently learn predictive models has a long history spanning Bayesian experimental design, active learning, and Bayesian optimization. While these areas have often evolved under different terminologies and objectives, they share a common Bayesian decision-theoretic foundation: the use of probabilistic surrogate models and utility-driven data acquisition to reduce epistemic uncertainty. Typically, the probabilistic surrogate is constructed by conditioning on the observations gathered so far, and the next experiment determined by optimizing an acquisition function given the surrogate (Di Fiore et al., 2024).

This section briefly surveys Bayesian experimental design, active learning, and Bayesian optimization, emphasizing that they primarily differ in the choice of latent target and utility function, rather than in their fundamental principles. We then focus on the probabilistic surrogate model that underlies most modern instantiations of these frameworks: Gaussian process regression.

**Bayesian Experimental Design.** Bayesian experimental design formalizes data acquisition as the maximization of expected utility under a probabilistic model (Bernardo, 1979). Early foundational work by Lindley (1956) introduced expected information gain (EIG) as a principled de-

sign criterion, defined as the conditional mutual information  $EIG(\mathbf{x}) := \mathcal{I}(\mathbf{z}; \mathbf{y} \mid \mathbf{x})$ , measuring the expected reduction in uncertainty about latent variables  $\mathbf{z}$  induced by observing outcomes  $\mathbf{y}$  from experiment  $\mathbf{x}$ . There are several ways of rewriting the EIG (Rainforth et al., 2024), with different implications for inference. The most common is

$$EIG(\mathbf{x}) = \mathbb{E}_{p(\mathbf{z})p(\mathbf{y} \mid \mathbf{x}, \mathbf{z})} [\log p(\mathbf{z} \mid \mathbf{x}, \mathbf{y}) - \log p(\mathbf{z})], \quad (1)$$

where  $p(\mathbf{z})$  is the prior, which is usually assumed to be independent of the experiment  $\mathbf{x}$ , and the likelihood  $p(\mathbf{y} \mid \mathbf{x}, \mathbf{z})$  can be interpreted as a simulator of experiment outcomes given  $\mathbf{x}$  and  $\mathbf{z}$ .

In sequential Bayesian experimental design, also called Bayesian adaptive design, one typically considers the current posterior as the prior for the next iteration.

**Active Learning for Regression.** In machine learning, active learning is often a computationally motivated instantiation of sequential design, targeting settings where a large unlabeled dataset exists and the goal is to identify the most informative ones to label (Liu et al., 2022). Although much of the active learning literature focuses on classification (Settles, 2009), MacKay (1992) introduced Bayesian active learning through information-theoretic criteria for regression models, showing that data selection based on posterior uncertainty can dramatically improve sample efficiency. Housley et al. (2011) targets information gain in model parameters but uses the symmetry of conditional mutual information,  $\mathcal{I}(\mathbf{z}; \mathbf{y} \mid \mathbf{x}) = \mathcal{I}(\mathbf{y}; \mathbf{z} \mid \mathbf{x})$ , to rewrite the EIG such that entropies are computed in the (usually low-dimensional) output space,

$$EIG(\mathbf{x}) = H[\mathbf{y} \mid \mathbf{x}] - \mathbb{E}_{p(\mathbf{z})} [H[\mathbf{y} \mid \mathbf{x}, \mathbf{z}]]. \quad (2)$$

Since this is maximized by the experiments  $\mathbf{x}$  where predictions disagree most across  $\mathbf{z}$ , this approach is called Bayesian active learning by disagreement (BALD) (Housley et al., 2011). However, Bickford Smith et al. (2023) show

that reducing parameter uncertainty does not necessarily improve predictive performance, arguing that if the target input distribution is fixed, one should instead target downstream predictive uncertainty directly.

**Bayesian Optimization.** Bayesian optimization (BO) is commonly presented as a framework for global optimization of expensive black-box functions (Garnett, 2023). From a design perspective, BO can be interpreted as an adaptive experimental design, where the latent quantity of interest is the function optimum rather than the full predictive surface. Information-theoretic BO methods, such as entropy search (Hennig & Schuler, 2012), make this connection explicit by selecting evaluations that maximize the reduction in posterior uncertainty over the optimizer.

**Gaussian processes.** Throughout this work, we use a Gaussian process (GP) prior on the latent variable  $z$ ,

$$z \sim \mathcal{GP}(m(\mathbf{x}), k_\theta(\mathbf{x}, \mathbf{x}')), \quad (3)$$

meaning that for any finite set of inputs  $X = \{\mathbf{x}_i\}_{i=1}^N$ , the function values  $\mathbf{z}(X) = (z(\mathbf{x}_1), \dots, z(\mathbf{x}_N))^\top$  are jointly Gaussian. Here  $m(\mathbf{x})$  denotes the mean function and  $k_\theta(\mathbf{x}, \mathbf{x}')$  a positive definite covariance kernel with hyperparameters  $\theta$ . We further assume the observations to be corrupted by independent Gaussian noise,

$$y_i = z(\mathbf{x}_i) + \varepsilon_i, \quad \varepsilon_i \sim \mathcal{N}(0, \sigma_n^2), \quad (4)$$

and write  $\mathbf{y} = (y_1, \dots, y_N)^\top$  and  $\mathcal{D} = \{X, \mathbf{y}\}$ . Let  $K \in \mathbb{R}^{N \times N}$  denote the kernel matrix with  $K_{ij} = k_\theta(\mathbf{x}_i, \mathbf{x}_j)$ , and let  $\mathbf{k}_* = (k_\theta(\mathbf{x}_1, \mathbf{x}_*), \dots, k_\theta(\mathbf{x}_N, \mathbf{x}_*))^\top$ . Then the predictive posterior at a test input  $\mathbf{x}_*$  is Gaussian,

$$p(z_* | \mathcal{D}, \mathbf{x}_*) = \mathcal{N}(\mu(\mathbf{x}_*), s^2(\mathbf{x}_*)),$$

with mean and variance given in closed form by

$$\mu(\mathbf{x}_*) = m(\mathbf{x}_*) + \mathbf{k}_*^\top (K + \sigma_n^2 I)^{-1} (\mathbf{y} - m(X)), \quad (5)$$

$$s^2(\mathbf{x}_*) = k_\theta(\mathbf{x}_*, \mathbf{x}_*) - \mathbf{k}_*^\top (K + \sigma_n^2 I)^{-1} \mathbf{k}_*. \quad (6)$$

Under this GP model, the expected information gain in  $z$  from an experiment  $\mathbf{x}_*$  follows from the BALD formulation in equation (2) after noting that the differential entropy of a univariate Gaussian  $\mathcal{N}(\mu, \sigma^2)$  is  $H = 0.5 \log 2\pi e \sigma^2$ . Specifically,

$$H[y_* | \mathcal{D}, \mathbf{x}_*] = 0.5 \log 2\pi e (s^2(\mathbf{x}_*) + \sigma_n^2) \quad (7)$$

since  $p(y_* | \mathcal{D}, \mathbf{x}_*) = \mathcal{N}(\mu(\mathbf{x}_*), s^2(\mathbf{x}_*) + \sigma_n^2)$ .

Further conditioning on a particular realization  $z_*$  leaves only observation noise,  $p(y_* | \mathcal{D}, \mathbf{x}_*, z_*) = \mathcal{N}(z_*, \sigma_n^2)$ , hence

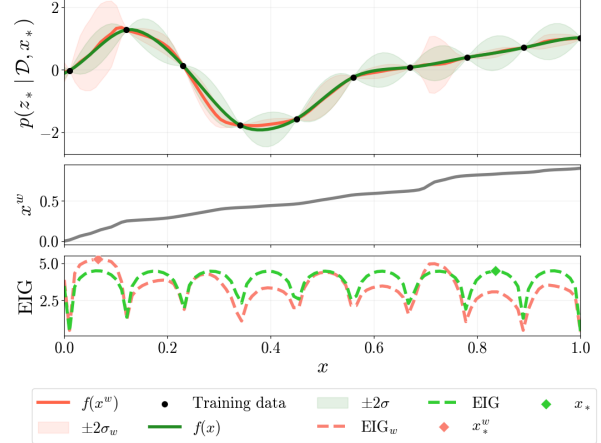


Figure 2. Predictive distribution and EIG for a warped and unwarped GP. The middle figure shows the warped  $x^w$ , using rational quadratic splines, relative to the unwarped  $x$ .

$$\mathbb{E}_{z_*} [H[y_* | \mathbf{x}_*, z_*]] = 0.5 \log 2\pi e \sigma_n^2 \quad (8)$$

Combining equations (7) and (8) gives

$$\text{EIG}(\mathbf{x}_*) = 0.5 \log 2\pi e \left( \frac{s^2(\mathbf{x}_*) + \sigma_n^2}{\sigma_n^2} \right). \quad (9)$$

Importantly, this shows that the expected information gain only depends on the posterior variance and not the mean. Belakaria et al. (2024) show that this conclusion extends to other variance-based acquisition functions, as well as ones targeting the gradient of a Gaussian process.

**Non-stationary Gaussian processes.** Most Gaussian process models assume stationarity, which can limit performance on complex, real-world data. To model non-stationary functions, (Snelson et al., 2003; Lázaro-Gredilla, 2012) first proposed *output*-warped GPs to handle non-Gaussian noise distributions. Later, Snoek et al. (2014) introduced *input*-warped Gaussian Processes, utilizing monotonic Beta CDFs to map inputs to a latent stationary space. Non-stationarity can also be achieved through hierarchical constructions, such as treating the output of one GP as the input to another GP (Damianou & Lawrence, 2013; Sauer et al., 2023), or putting GP priors on the hyperparameters (Heinonen et al., 2016; Zhao et al., 2021).

### 3. Methodology

Variance-based acquisition functions depend only on the surrogate model’s predictive variance. For stationary Gaussian processes, this variance is evaluated with respect to a fixed input geometry and, conditional on the hyperparameters, is independent of observed function values. Exploration is thus driven by the distribution of sampled inputs rather than by the structure in the observations.

We learn an input reparameterization that modifies this geometry for acquisition while leaving the predictive Gaussian process unchanged.

Throughout, we consider variance-based acquisition functions, such as expected information gain, that depend exclusively on the GP predictive variance. This perspective motivates treating the input geometry itself as the object of adaptation. In practice, surrogate hyperparameters and the warp are updated alternately during sequential acquisition.

### 3.1. Input-warped Gaussian processes

Having identified that variance-based acquisition under a fixed surrogate geometry does not directly condition on observed responses, we introduce a mechanism that allows data to influence exploration by reshaping the input geometry itself. Specifically, we define a nonlinear reparameterization of the input space via a bijective mapping  $T_\phi : \mathcal{X} \rightarrow \mathcal{X}^w$ , and instantiate a Gaussian process in the warped coordinates  $\mathbf{x}^w = T_\phi(\mathbf{x})$ ,

$$z \sim \mathcal{GP}(m(\mathbf{x}^w), k_\theta(\mathbf{x}^w, \mathbf{x}^w)). \quad (10)$$

The warp  $T_\phi$  is parameterized as a smooth, injective map, so that the input space is reparameterized without foldings or self-intersections. This ensures that distances under the kernel remain well defined and preserve their standard interpretation in terms of covariance and predictive uncertainty. Although the warp is a deterministic function of  $\mathbf{x}$ , its parameters  $\phi$  are learned from the observed data  $\mathcal{D} = \{\mathbf{X}, \mathbf{y}\}$ . It therefore rescales distances in the input space in a data-dependent manner. Since variance-based acquisition criteria depend monotonically on the GP predictive variance, this rescaling directly shapes the acquisition landscape while the predictive GP model itself remains fixed, as illustrated in Figure 2. The overall procedure is outlined in Algorithm 1.

### 3.2. Warp parameterization

We parameterize the input warp  $T_\phi$  using monotone spline transformations from the normalizing flow literature (Durkan et al., 2019; Papamakarios et al., 2021). These maps are smooth and injective by construction, providing a flexible reparameterization of the input space without foldings. When applied at the input geometry level, the warp induces non-stationarity while preserving standard Gaussian process inference.

Similar input transformations have been used in deep kernel learning (Wilson et al., 2016; Al-Shedivat et al., 2017) and manifold Gaussian processes (Calandra et al., 2016) to increase model expressivity. Here, the warp is instead used exclusively to reshape the geometry underlying the acquisition function.

We instantiate  $T_\phi : [0, 1]^D \rightarrow [0, 1]^D$  using conditional

---

**Algorithm 1** Input-warped Bayesian active learning

---

**Input:**  $\mathcal{X}$ , noisy oracle  $f(\mathbf{x})$ , surrogate model  $\mathcal{GP}$ , warp  $T_\phi$ , acquisition function  $\alpha(\mathbf{x}, \mathcal{GP})$ , budget  $B$ .

**Output:**  $\mathcal{D}_B, \mathcal{GP}$ .

- 1: Initialize data  $\mathcal{D}_0$  with  $b_0$  starting observations.
- 2: **for** each iteration  $i \in [b_0 + 1, B]$  **do**
- 3:     Fit the  $\mathcal{GP}$  parameters  $\theta$ , with  $\phi$  frozen.
- 4:     Fit the warp parameters  $\phi$ , with  $\theta$  frozen.
- 5:     Select the next experiment point by maximizing the acquisition function:

$$\mathbf{x}_* \leftarrow \arg \max_{\mathbf{x} \in \mathcal{X}} \alpha(T_\phi(\mathbf{x}), \mathcal{GP}(\mathcal{D}_{i-1}))$$

- 6:     Observe  $y_* = f(\mathbf{x}_*)$ .
- 7:     Update data  $\mathcal{D}_i = \mathcal{D}_{i-1} \cup \{(\mathbf{x}_*, y_*)\}$ .
- 8: **end for**

---

rational quadratic splines (C-RQS). The construction follows the standard coupling-layer formulation: in each layer, spline parameters for a subset of dimensions are predicted as functions of the remaining dimensions, which are left unchanged. The full warp is obtained by composing multiple such coupling layers with alternating partitions. Each layer applies strictly monotone one-dimensional spline mappings, ensuring global injectivity and preserving the interpretation of kernel distances. Further details on the spline construction are given in Appendix A.2.

### 3.3. Training the warp

The parameters  $\phi$  of the input warp are trained using objectives that act on the geometry induced by the Gaussian process posterior. Throughout, the predictive GP model and its hyperparameters are kept fixed; the warp is used only to modify the input space in which predictive variances are evaluated for acquisition.

Given observed inputs  $X = \{\mathbf{x}_i\}_{i=1}^N$  and responses  $y$ , we define a warped kernel

$$k_{\theta, \phi}(\mathbf{x}, \mathbf{x}') = k_\theta(T_\phi(\mathbf{x}), T_\phi(\mathbf{x}')). \quad (11)$$

This kernel is used exclusively for computing predictive variances within the acquisition function. All reported predictions and evaluation metrics are obtained from the unwarped GP.

**Self-supervised objective.** Our primary training objective for the warp is a self-supervised loss that globally regularizes the induced posterior geometry over the domain. To achieve this, we employ a fixed reference model—a standard GP with an identity warp—to serve as a geometric anchor. Crucially, this reference model is not used for acquisition or final prediction, only providing a stable target for optimizing the warp parameters.

We sample a set of probe locations  $\mathcal{U} = \{\mathbf{u}_m\}_{m=1}^M$  quasi-randomly over  $\mathcal{X}$  using a Sobol sequence and evaluate the reference (non-warped) posterior mean  $\mu_{\text{ref}}(\mathbf{u})$  at these locations. At each probe location, the warped kernel induces a posterior mean  $\mu_\phi(\mathbf{u})$  and variance  $s_\phi^2(\mathbf{u})$ . We fit the warp parameters by minimizing the expected negative log predictive density of the reference mean under the warped posterior using AdamW (Loshchilov & Hutter, 2019),

$$\mathcal{L}_w(\phi) = \mathbb{E}_{\mathbf{u} \sim \mathcal{U}} [-\log \mathcal{N}(\mu_{\text{ref}}(\mathbf{u}) \mid \mu_\phi(\mathbf{u}), s_\phi^2(\mathbf{u}) + \sigma^2)]. \quad (12)$$

Note that this only requires gradients with respect to  $\phi$ .

This objective is not intended to improve predictive accuracy. Instead, it regularizes the uncertainty structure induced by the warped kernel away from the observed inputs. By redistributing predictive variance across the domain, the warp allows variance-based acquisition functions to allocate exploration budget preferentially to regions that are poorly explained by the current model, including regions of rapid local variation, while leaving the predictive GP model unchanged.

**Marginal log-likelihood.** For comparison, we also consider training the warp parameters  $\phi$  by maximizing the marginal log-likelihood (MLL) of the Gaussian process under the warped kernel. Given observations  $\mathcal{D} = \{X, \mathbf{y}\}$ , this objective is

$$\log p(\mathbf{y} \mid X, \phi) = -\frac{1}{2}\mathbf{y}^\top K_\phi^{-1}\mathbf{y} - \frac{1}{2}\log|K_\phi| - \frac{N}{2}\log 2\pi, \quad (13)$$

where  $K_\phi = K(T_\phi(X), T_\phi(X)) + \sigma_n^2 I$ . When optimizing this objective, all GP hyperparameters are held fixed and gradients are taken only with respect to  $\phi$ .

While MLL provides a principled likelihood-based training signal, it constrains the warp only through kernel evaluations at the observed input locations. As a result, it offers limited control over the induced geometry in unobserved regions, which is critical for variance-based acquisition.

### 3.4. Related work

In the Bayesian optimization literature, Bodin et al. (2020) proposed injecting noise into the input of a Gaussian process to disregard overly complex behaviour of the function being optimized. However, in this work, our aim is exactly the opposite: sampling *more* where the function is complex. Belakaria et al. (2024) studied several acquisition functions based on derivative-based global sensitivity but concluded that efficient gradient estimation mandates sampling close to previous inputs, which runs counter to the intuition of efficient exploration. More similar to us, McHutchon & Rasmussen (2011) show that input noise translates to output noise that depends on the gradient magnitude, thereby guiding the design toward high-complexity regions.

## 4. Experiments

### 4.1. Baselines

We compare against three baselines designed to isolate different aspects of the proposed method. First, we include an unwarped Gaussian process, representing standard variance-based acquisition under a stationary surrogate. Second, we consider a globally monotone input warp based on the Kumaraswamy cumulative distribution function (Snoek et al., 2014), further described in Appendix A.1. This transformation provides a low-dimensional, global reparameterization of the input space but lacks the expressivity required to capture localized non-stationarity. Finally, we evaluate the proposed conditional rational quadratic spline (C-RQS) warp, trained either by marginal log-likelihood or using the self-supervised objective in equation (12).

### 4.2. Evaluation metrics

We evaluate predictive performance using mean squared error (MSE), which measures pointwise accuracy, and the continuous ranked probability score (CRPS), which assesses the quality of the full predictive distribution. CRPS is particularly relevant in active learning, as it penalizes both biased predictions and miscalibrated uncertainty. Lower values indicate better performance.

$$\text{CRPS} = \int_{\mathbb{R}} [F(t) - \mathbb{I}(t \geq y)]^2 dt. \quad (14)$$

In addition, we evaluate the derivative of the posterior mean, which is available in closed form for Gaussian processes with differentiable kernels. This serves as a diagnostic tool for determining whether the surrogate captures the local structure of the target function, including the placement of steep transitions, and it complements the scalar error metrics mentioned above.

### 4.3. Experimental setup

All input domains are affinely rescaled to  $[0, 1]^D$  prior to modeling, ensuring that the spline-based warp is well-defined.

All Gaussian process models use a Matérn 5/2 kernel with automatic relevance determination, where each input dimension is associated with a separate lengthscale  $\ell_i$ . Distances are computed as  $r^2 = \sum_{i=1}^D (x_i - x'_i)^2 / \ell_i^2$ . Additional hyperparameters include the signal variance  $\sigma_f^2$  and the observation noise variance  $\sigma_n^2$ , both learned during GP training.

Synthetic observations are corrupted by additive Gaussian noise with a standard deviation of 0.05  $\text{std}(f)$  during acquisition, with the noise variance not revealed to the Gaussian process.

For a  $D$ -dimensional problem, we initialize the surrogate

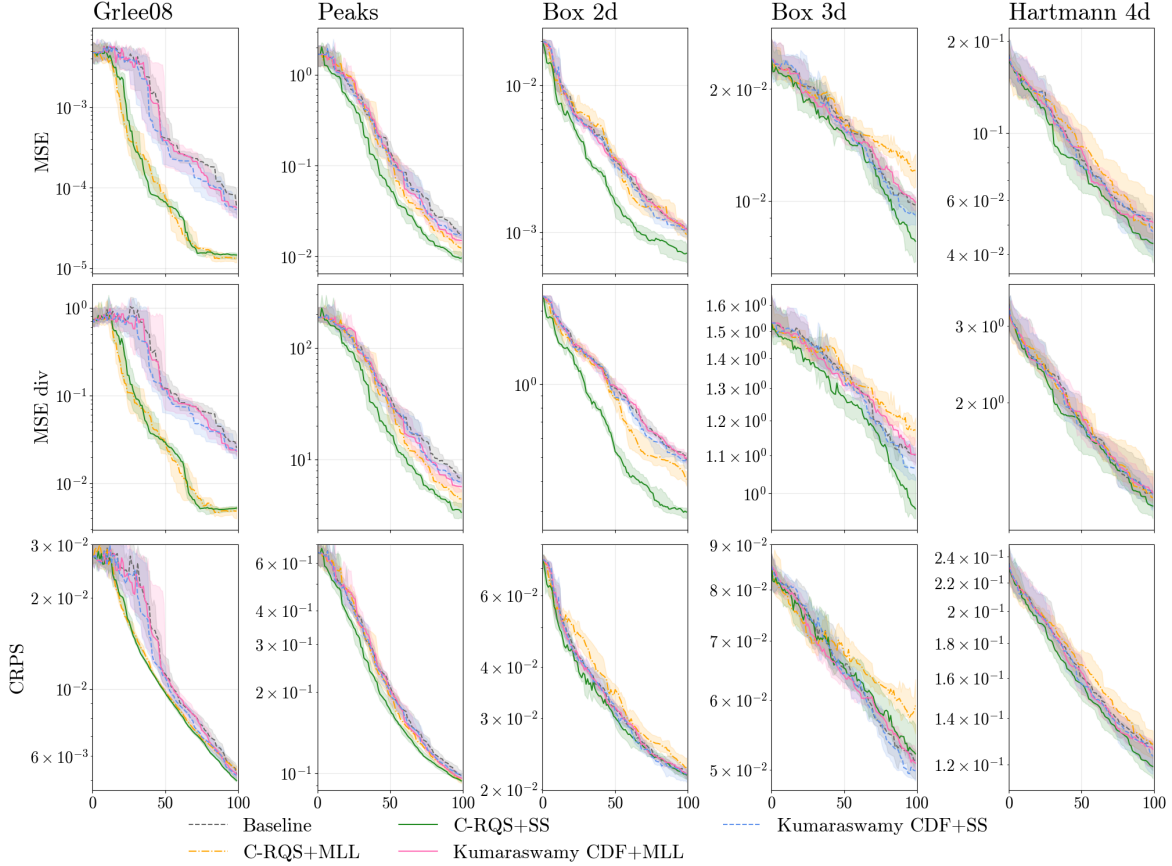


Figure 3. Average relative decrease in each performance metric on the synthetic benchmark functions Gramacy-Lee08 ( $D = 2$ ), Peaks ( $D = 2$ ), Box ( $D = 2, 3$ ) and Hartmann ( $D = 4$ ). In all tasks our proposed C-RQS warp achieves superior performance, with four out five cases trained in a self-supervised (SS) fashion.

with  $10 \times D$  Sobol samples. We then perform sequential acquisition using the EIG with a fixed budget of 100 evaluations. All results are averaged over 10 independent runs with different random initializations. The Gaussian processes are implemented in GPyTorch (Gardner et al., 2018), and the optimization of the acquisition function in PyTorch (Paszke et al., 2019). Further details on the training are provided in Appendix B.

#### 4.4. Synthetic benchmark functions

We evaluate performance on a collection of standard synthetic benchmark functions in 2, 3, and 4 dimensions: Gramacy–Lee08 and MATLAB Peaks ( $D = 2$ ), a smooth box function ( $D = 2, 3$ , see Appendix C), and the Hartmann function ( $D = 3, 4$ ). These functions exhibit varying degrees of non-stationarity and local structure.

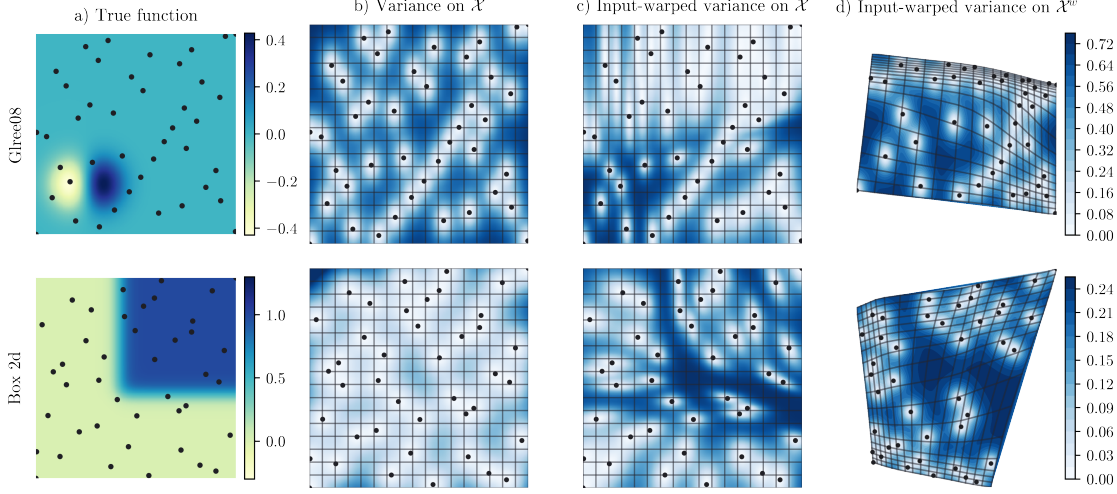
##### 4.4.1. RESULTS AND ANALYSIS

Figure 3 shows the evolution of predictive performance over the number of acquired points for five benchmark functions.

Across all benchmarks, the self-supervised RQS warp consistently improves sample efficiency relative to both the unwarped GP and likelihood-trained warps.

On the Gramacy–Lee08 function, training the warp via marginal likelihood also yields competitive performance, suggesting that likelihood-based objectives can be sufficient in settings with relatively smooth or homogeneous structures. In contrast, on functions exhibiting stronger local variation, marginal likelihood training is often unstable and can perform worse than not using a warp at all. This behavior highlights the limited ability of likelihood-based objectives to control the induced geometry in regions away from the observed inputs.

Figure 3 compares the relative decrease in MSE, CRPS, and mean-derivative error as a function of the number of acquired points. Across all test functions, input warping improves performance over standard GPs, with the largest gains observed for the proposed self-supervised C-RQS warp. In higher dimensions, differences among warping strategies are less pronounced at early iterations but become increasingly significant as additional data is acquired.



**Figure 4.** Illustrative example of geometry-aware Gaussian process modeling on synthetic two-dimensional benchmark functions. Results are shown for the GLREE08 function (top row) and the Box-2D function (bottom row). (a) Ground-truth function evaluated on a dense grid, together with the current set of training points. (b) Predictive variance of a standard Gaussian process in the original input space, reflecting uncertainty induced primarily by sparse sampling. (c) Predictive variance of the input-warped Gaussian process evaluated in the original input space (pullback), illustrating how the learned geometry redistributes uncertainty toward regions of localized variation. (d) The same predictive variance visualized in the warped input space, together with the deformed input mesh and warped training points. (e) Deformation of the two-dimensional input domain induced by the learned warp, demonstrating how resolution is adaptively concentrated in regions where the target function exhibits rapid local changes.

Table 1 reports the decrease in area relative to the baseline, where a positive value signifies an improvement over the baseline. The area reduction is calculated similarly to [Riis et al. \(2022\)](#); [Van Kempen & Van Vliet \(2000\)](#), for further details see Appendix D. The majority of all input warped trials achieve better performance than the baseline, and the best performing method for all functions in the metrics MSE and CRPS are highlighted in bold.

#### 4.5. Real-world example: mapping solar cell properties

We further evaluate the proposed warped Gaussian process framework on real-world datasets for solar cell characterization. The dataset is taken from [Rudisch et al. \(2020\)](#), and contains the intensity of the photoluminescence signal mapped across the surface of a thin film of a solar cell material. Composition gradients across the sample result in a distribution of the signal. Regions of rapid change are of special interest since they are associated with phase boundaries. Although this is a static dataset, such mapping could also be performed in an active learning scenario.

To resemble the experimental dataset, we used a standard GP simulator to model the function used as ground truth. An initial design of 20 points is chosen using farthest-point sampling to ensure spatial coverage, followed by sequential acquisition using EIG.

All models use, as before, a stationary Gaussian process surrogate with a Matérn 5/2 kernel and automatic relevance

determination. As before, the learned input warp is applied *only* within the acquisition function; predictive performance is always evaluated using the unwarped GP. Warp parameters are trained using the proposed self-supervised geometric objective. Since noise-free targets are unavailable, performance is assessed using CRPS, computed on the observation predictive distribution  $p(y_* | x_*, \mathcal{D})$ .

Figure 5 shows the predictive performance over the number of acquired points for two real-world photoluminescence datasets (IA & IB) in the two-dimensional input space (corresponding to spatial coordinates). Across all tasks, the self-supervised C-RQS warp achieves superior performance over both the standard GP and mll-trained warps.

#### 4.6. Limitations

While the proposed framework improves sample efficiency in non-stationary settings, it operates under several scope limitations. First, we focus on the small-data regime typical of experimental design, using relatively low-capacity predictive models with low-to-moderate input dimensions ( $D \leq 4$ ). Learning expressive warp parameterizations in higher dimensions from sparse data remains an open challenge: as dimensionality increases, the data required to infer a meaningful geometric transformation may negate the gains in sample efficiency. Second, although the warp can represent sharp transitions by locally expanding the input space, it cannot capture true discontinuities without introducing

Table 1. Percent reduction in area under the curve relative to the baseline (larger is better). The best performing method for all functions is highlighted. We find that, in most cases, a self-supervised (SS) trained C-RQS warp yields the greatest area reduction.

Model (%)	Grlee08		Peaks		Box 2d		Box 3d		Hartmann 4d	
	MSE	CRPS	MSE	CRPS	MSE	CRPS	MSE	CRPS	MSE	CRPS
Kumaraswamy + SS	8.76 ± 0.21	4.23 ± 0.04	6.79 ± 0.13	2.73 ± 0.02	2.54 ± 0.01	0.86 ± 0.00	1.68 ± 0.01	0.50 ± 0.00	1.91 ± 0.01	0.62 ± 0.00
C-RQS + MLL	<b>52.36 ± 0.55</b>	16.85 ± 0.13	9.51 ± 1.52	4.46 ± 0.21	1.63 ± 0.04	-5.24 ± 0.02	-6.36 ± 0.10	-4.64 ± 0.02	-2.24 ± 0.04	-1.69 ± 0.01
Kumaraswamy + MLL	-0.16 ± 1.16	0.21 ± 0.19	6.23 ± 0.53	2.19 ± 0.09	1.66 ± 0.03	0.78 ± 0.00	0.42 ± 0.00	<b>0.68 ± 0.00</b>	0.98 ± 0.01	0.31 ± 0.00
C-RQS + SS	47.92 ± 0.25	<b>17.64 ± 0.07</b>	<b>29.00 ± 0.45</b>	<b>13.4 ± 0.09</b>	<b>29.28 ± 0.05</b>	<b>5.10 ± 0.01</b>	<b>5.65 ± 0.10</b>	-1.33 ± 0.02	<b>9.58 ± 0.03</b>	<b>3.40 ± 0.00</b>

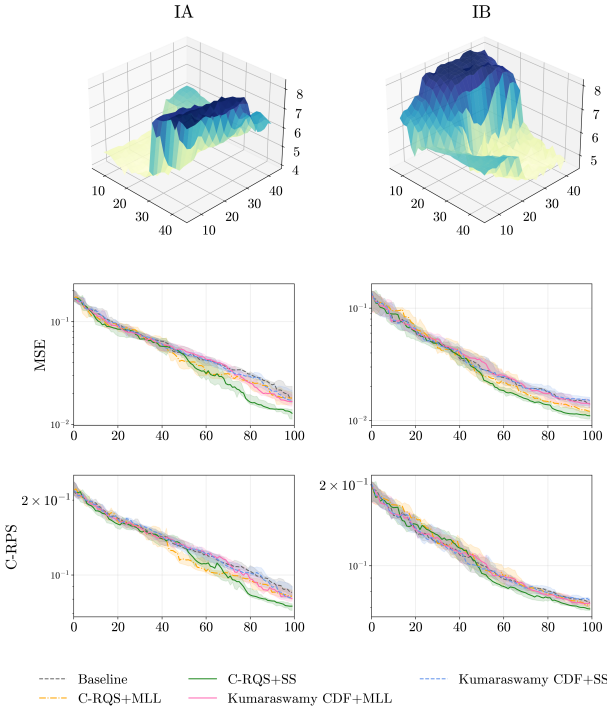


Figure 5. Average relative decrease in each performance metric on two photoluminescence datasets (IA & IB shown to the left). Our proposed method C-RQS trained via self-supervised learning achieves superior performance across all tasks.

extreme distortions.

## 5. Discussion

A central insight of this work is that the effectiveness of variance-based acquisition functions is governed not only by the uncertainty model but also by the geometry in which that uncertainty is measured. In a stationary Gaussian process, the predictive variance is evaluated with respect to a fixed input metric and is insensitive to observed function values once the hyperparameters are fixed. As a result, exploration strategies based purely on variance operate in an essentially open-loop manner: they adapt to input locations but not to structural information revealed by the data.

By learning an input reparameterization that reshapes this geometry, we introduce a controlled form of feedback into the exploration process via the induced input metric. Re-

gions of the domain can be expanded or compressed in response to observed variability, directly modulating predictive uncertainty without modifying the underlying predictive model. Our results suggest that improving active learning performance does not necessarily require more expressive surrogate models; instead, substantial gains can be achieved by rethinking the geometry used to measure uncertainty rather than the uncertainty model itself.

We emphasize that the primary objective of the proposed method is adaptive data collection. The acquisition geometry is decoupled from the predictive model, and the surrogate function is returned only as a byproduct; any downstream model can then be trained for tasks such as regression.

Recent work on high-dimensional Bayesian optimization argues that appropriate rescaling of the length scales, for instance through a lognormal hyperprior, can lead to drastic performance improvements (Hvafner et al., 2024). Understanding the relationship between such implicit geometric adaptations and the explicit learned reparameterizations considered here remains an interesting direction for future work.

## 6. Conclusions

Active learning is commonly framed as a problem of uncertainty modeling. This work highlights that it is equally a problem of geometry. We show that by learning a non-linear reparameterization of the input space, variance-based acquisition can respond to structure revealed by the data, introducing feedback into an otherwise open-loop exploration process. Decoupling the acquisition geometry from the predictive model allows exploration to concentrate on regions of high variability without compromising inference. In practice, a geometric self-supervised objective is more appropriate for this purpose than marginal likelihood maximization, leading to improved sample efficiency on both synthetic benchmarks and a real-world dataset in non-stationary settings. The broader implication is that improved active learning does not require increasingly expressive surrogate models. Instead, gains arise from treating the input geometry itself as a design choice for exploration.

## Acknowledgements

This work is supported by the Swedish Foundation for Strategic Research (SSF), the strategic research area STandUP for Energy, the Wallenberg AI, Autonomous Systems and Software Program (WASP) funded by the Knut and Alice Wallenberg Foundation. The work used the National Academic Infrastructure for Super computing in Sweden (NAIIS).

## Impact Statement

This paper presents work whose goal is to advance the field of Machine Learning. There are many potential societal consequences of our work, none which we feel must be specifically highlighted here.

## References

Al-Shedivat, M., Wilson, A. G., Saatchi, Y., Hu, Z., and Xing, E. P. Learning scalable deep kernels with recurrent structure. *Journal of Machine Learning Research*, 18(82): 1–37, 2017.

Balandat, M., Karrer, B., Jiang, D. R., Daulton, S., Letham, B., Wilson, A. G., and Bakshy, E. BoTorch: A Framework for Efficient Monte-Carlo Bayesian Optimization. In *Advances in Neural Information Processing Systems* 33, 2020.

Belakaria, S., Letham, B., Doppa, J. R., Engelhardt, B., Ermon, S., and Bakshy, E. Active learning for derivative-based global sensitivity analysis with Gaussian processes. *Advances in Neural Information Processing Systems*, 37: 53887–53917, 2024.

Bernardo, J. M. Expected information as expected utility. *the Annals of Statistics*, pp. 686–690, 1979.

Bickford Smith, F., Kirsch, A., Farquhar, S., Gal, Y., Foster, A., and Rainforth, T. Prediction-oriented Bayesian active learning. In *International conference on artificial intelligence and statistics*, pp. 7331–7348. PMLR, 2023.

Bodin, E., Kaiser, M., Kazlauskaitė, I., Dai, Z., Campbell, N., and Ek, C. H. Modulating surrogates for Bayesian optimization. In *International Conference on Machine Learning*, pp. 970–979. PMLR, 2020.

Calandra, R., Peters, J., Rasmussen, C. E., and Deisenroth, M. P. Manifold gaussian processes for regression. In *2016 International joint conference on neural networks (IJCNN)*, pp. 3338–3345. IEEE, 2016.

Damianou, A. and Lawrence, N. D. Deep Gaussian processes. In *Artificial intelligence and statistics*, pp. 207–215. PMLR, 2013.

Di Fiore, F., Nardelli, M., and Mainini, L. Active learning and Bayesian optimization: A unified perspective to learn with a goal. *Archives Of Computational Methods in Engineering*, pp. 1–29, 2024.

Durkan, C., Bekasov, A., Murray, I., and Papamakarios, G. Neural spline flows. *Advances in neural information processing systems*, 32, 2019.

Gardner, J., Pleiss, G., Weinberger, K. Q., Bindel, D., and Wilson, A. G. GPYtorch: Blackbox matrix-matrix Gaussian process inference with GPU acceleration. *Advances in neural information processing systems*, 31, 2018.

Garnett, R. *Bayesian optimization*. Cambridge University Press, 2023.

Ghavamzadeh, M., Mannor, S., Pineau, J., Tamar, A., et al. Bayesian reinforcement learning: A survey. *Foundations and Trends® in Machine Learning*, 8(5-6):359–483, 2015.

Heinonen, M., Mannerström, H., Rousu, J., Kaski, S., and Lähdesmäki, H. Non-stationary Gaussian process regression with Hamiltonian Monte Carlo. In *Artificial intelligence and statistics*, pp. 732–740. PMLR, 2016.

Hennig, P. and Schuler, C. J. Entropy search for information-efficient global optimization. *The Journal of Machine Learning Research*, 13(1):1809–1837, 2012.

Houlsby, N., Huszár, F., Ghahramani, Z., and Lengyel, M. Bayesian active learning for classification and preference learning. *arXiv preprint arXiv:1112.5745*, 2011.

Hvarfner, C., Hellsten, E. O., and Nardi, L. Vanilla Bayesian optimization performs great in high dimensions. In *International Conference on Machine Learning (ICML)*, 2024.

Jarl, S., Sjölund, J., Frost, R. J., Holst, A., and Scragg, J. J. Machine learning for in-situ composition mapping in a self-driving magnetron sputtering system. *Materials & Design*, 260:115087, 2025.

Krause, A. and Guestrin, C. Nonmyopic active learning of Gaussian processes: an exploration-exploitation approach. In *Proceedings of the 24th international conference on Machine learning*, pp. 449–456, 2007.

Krause, A., Singh, A., and Guestrin, C. Near-optimal sensor placements in Gaussian processes: Theory, efficient algorithms and empirical studies. *Journal of Machine Learning Research*, 9(2), 2008.

Lázaro-Gredilla, M. Bayesian warped gaussian processes. *Advances in Neural Information Processing Systems*, 25, 2012.

Lindley, D. V. On a measure of the information provided by an experiment. *The Annals of Mathematical Statistics*, 27 (4):986–1005, 1956.

Liu, P., Wang, L., Ranjan, R., He, G., and Zhao, L. A survey on active deep learning: From model driven to data driven. *ACM Computing Surveys (CSUR)*, 54(10s):1–34, 2022.

Loshchilov, I. and Hutter, F. Decoupled weight decay regularization. In *International Conference on Learning Representations (ICLR)*, 2019.

MacKay, D. J. Information-based objective functions for active data selection. *Neural computation*, 4(4):590–604, 1992.

McHutchon, A. and Rasmussen, C. Gaussian process training with input noise. *Advances in neural information processing systems*, 24, 2011.

Papamakarios, G., Nalisnick, E., Rezende, D. J., Mohamed, S., and Lakshminarayanan, B. Normalizing flows for probabilistic modeling and inference. *Journal of Machine Learning Research*, 22(57):1–64, 2021.

Paszke, A., Gross, S., Massa, F., Lerer, A., Bradbury, J., Chanan, G., Killeen, T., Lin, Z., Gimelshein, N., Antiga, L., et al. PyTorch: An imperative style, high-performance deep learning library. *Advances in neural information processing systems*, 32, 2019.

Rainforth, T., Foster, A., Ivanova, D. R., and Bickford Smith, F. Modern Bayesian experimental design. *Statistical Science*, 39(1):100–114, 2024.

Rasmussen, C. E. and Williams, C. K. *Gaussian processes for machine learning*, volume 2. MIT press Cambridge, MA, 2006.

Riis, C., Antunes, F., Hüttel, F., Lima Azevedo, C., and Pereira, F. Bayesian active learning with fully bayesian gaussian processes. *Advances in Neural Information Processing Systems*, 35:12141–12153, 2022.

Rudisch, K., Davydova, A., Riekehr, L., Adolfsson, J., Casal, L. Q., Platzer-Björkman, C., and Scragg, J. Prospects for defect engineering in cu 2 znsns 4 solar absorber films. *Journal of Materials Chemistry A*, 8(31), 2020.

Sauer, A., Gramacy, R. B., and Higdon, D. Active learning for deep Gaussian process surrogates. *Technometrics*, 65 (1):4–18, 2023.

Settles, B. Active learning literature survey. Technical report, University of Wisconsin-Madison Department of Computer Sciences, 2009.

Snelson, E., Ghahramani, Z., and Rasmussen, C. Warped gaussian processes. *Advances in neural information processing systems*, 16, 2003.

Snoek, J., Swersky, K., Zemel, R., and Adams, R. Input warping for Bayesian optimization of non-stationary functions. In *International conference on machine learning*, pp. 1674–1682. PMLR, 2014.

Teixeira Parente, M., Brandl, G., Franz, C., Stuhr, U., Ganeva, M., and Schneidewind, A. Active learning-assisted neutron spectroscopy with log-Gaussian processes. *Nature Communications*, 14(1):2246, 2023.

Van Kempen, G. and Van Vliet, L. Mean and variance of ratio estimators used in fluorescence ratio imaging. *Cytometry: The Journal of the International Society for Analytical Cytology*, 39(4):300–305, 2000.

Wilson, A. G., Hu, Z., Salakhutdinov, R., and Xing, E. P. Deep kernel learning. In *Artificial intelligence and statistics*, pp. 370–378. PMLR, 2016.

Zhao, Z., Emzir, M., and Särkkä, S. Deep state-space Gaussian processes. *Statistics and Computing*, 31(6):75, 2021.

## A. Warp parameterizations

### A.1. Kumaraswamy warp

We use an input warp similar to the Beta distribution proposed by Snoek et al. (2014), namely the Kumaraswamy distribution as implemented in Balandat et al. (2020), which has a differentiable and closed-form CDF. It has two trainable parameters  $\phi = a, b$ , both positive, that control the concentration. It maps the unit interval onto itself.

$$T_\phi(x) = 1 - (1 - x^a)^b, \quad (15)$$

In higher dimensions ( $D \geq 2$ ), each input dimension is transformed using a separate warping function.

### A.2. Conditional Rational Quadratic Spline Warps

Here we summarize the rational quadratic spline (RQS) parameterization used to construct the input warp  $T_\phi$ . We focus on the structural properties required by the method; numerical details follow standard constructions (Durkan et al., 2019).

The warp  $T_\phi : [0, 1]^D \rightarrow [0, 1]^D$  is defined as a composition of monotone spline coupling transformations. Each coupling layer leaves a subset of input coordinates unchanged and transforms the remaining coordinates using one-dimensional rational quadratic splines conditioned on the unchanged subset.

Each layer is injective by construction, since transformed coordinates are strictly monotone functions of their own inputs for any fixed conditioning values. By stacking layers with alternating partitions, the resulting warp is globally injective and allows each output dimension to depend on all input dimensions.

#### A.2.1. MONOTONE RQS MAPPINGS

For a scalar input  $x \in [0, 1]$ , a rational quadratic spline defines a smooth, strictly monotone mapping  $g_\phi(x)$  by partitioning the domain into  $K$  bins with ordered knot locations. Within each bin, the mapping is defined by a rational quadratic function parameterized by bin widths, heights, and derivatives at the knots. Positivity constraints on these parameters ensure continuity and strict monotonicity.

In the conditional setting, spline parameters are predicted as functions of a conditioning input. For each transformed coordinate  $x_d$ , we define

$$g_{\phi_d}(x_d \mid \mathbf{x}_A),$$

where  $\mathbf{x}_A$  denotes the subset of coordinates left unchanged in the current coupling layer. Monotonicity is enforced uniformly over all conditioning values.

#### A.2.2. MULTI-DIMENSIONAL CONSTRUCTION

In each coupling layer, the input dimensions are partitioned into two disjoint sets,  $A$  and  $B$ . Coordinates in  $A$  are passed through unchanged, while coordinates in  $B$  are transformed independently via conditional RQS mappings:

$$y_A = x_A, \quad y_{B_j} = g_{\phi_j}(x_{B_j} \mid \mathbf{x}_A), \quad j \in B.$$

Since each transformation is strictly monotone in its corresponding input coordinate, the mapping is injective. Stacking such layers yields a flexible reparameterization without foldings or self-intersections. As the warp is used only to define an input geometry, the evaluation of the Jacobian determinant is not required.

## B. Optimization details

We alternate between (i) fitting the GP hyperparameters, (ii) updating the warp (when enabled), and (iii) optimizing the acquisition function to select the next query point.

### B.1. GP hyperparameter fitting

We fit the exact GP by maximizing the marginal log-likelihood using L-BFGS-B. Unless stated otherwise, the warp parameters are frozen during GP fitting (i.e., we optimize only kernel and likelihood parameters). We run L-BFGS-B for at most 300 iterations with tolerances  $10^{-6}$  (gradient) and  $10^{-9}$  (function value).

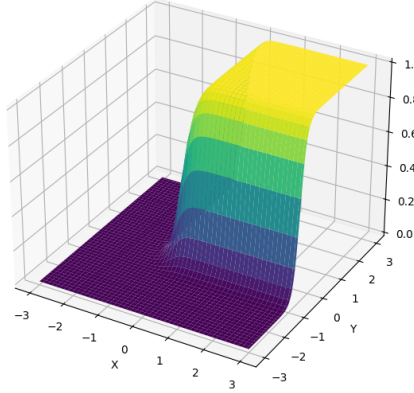


Figure 6. The smooth box test function with  $D = 2$  and smoothness parameter  $k = 7$ .

## B.2. Warp training

When a learnable warp is used, we optimize only the warp parameters  $\phi$  while keeping GP and likelihood parameters fixed. For the self-supervised variant, we form a frozen reference GP without warping and train  $\phi$  to match its posterior mean globally over the domain, using a negative log predictive density loss evaluated at  $M = 1024$  probe points sampled uniformly in the input space. We optimize  $\phi$  with AdamW (learning rate  $10^{-3}$ ) for 400 iterations, clip the warp gradient norm to 2, and decay the learning rate by a factor 0.5 every 50 steps.

## B.3. Acquisition optimization

At each round, we maximize the acquisition function with gradient-based optimization. We initialize 500 candidates using Latin hypercube sampling, optimize them jointly with L-BFGS for 300 steps (strong Wolfe line search), and return the best point.

## C. Smooth box function

We constructed a smooth box function to simulate possible real-world problems. In  $D$  dimensions, it is given by

$$f(\mathbf{x}) = \prod_{i=1}^d \sigma(k(x_i - b_{\text{start}})) (1 - \sigma(k(x_i - b_{\text{end}}))), \quad (16)$$

where  $\sigma$  represents a sigmoid function,  $k$  a smoothness parameter and  $b_{\text{start}}$  and  $b_{\text{end}}$  indicate the position of the box. In our implementation, we used  $k = 7$  and  $b_{\text{start}} = -0.5$  without an end point creating a plateau-like smooth step function.

## D. Area reduction

We compute the mean and variance of the relative decrease in area under the curve  $A_{\text{reduction}}$ , similar to Riis et al. (2022); Van Kempen & Van Vliet (2000). The unbiased estimates of the mean and variance of the ratio between the metric and the baseline in equation (17).

$$A_{\text{reduction}} = \frac{A_{\text{metric}} - A_{\text{baseline}}}{A_{\text{baseline}}} \quad (17)$$

If the area is computed by a metric that is not lower bounded, e.g., the negative marginal likelihood, all the areas should be subtracted by the best obtained performance across all the tested acquisition functions, to create an artificial lower bound. The unbiased estimate of the expectation of the area reduction can then be calculated according to

$$\mu_{\text{reduction}} = \frac{\mu_n}{\mu_d}, \quad (18)$$

where  $\mu_n$  and  $\mu_d$  are the expectations nominator and denominator of equation (17).

The unbiased estimate of the variance of the area reduction is

$$\sigma_{\text{reduction}}^2 = \frac{1}{R} \left( \frac{\sigma_n^2}{\mu_d^2} + \frac{\mu_n^2 \sigma_d^2}{\mu_d^4} - \frac{2\mu_n \sigma_{nd}^2}{\mu_d^3} \right) \quad (19)$$

where  $R$  is the number of times the acquisition function is run with different initial data sets,  $\sigma_n^2$ ,  $\sigma_d^2$ , and  $\sigma_{nd}^2$ , the variance of and covariance between the nominator and denominator.